EasyChair Preprint

№ 12524

Topology Optimization of Fiber Reinforced Composite Laminates for Minimum Structural Compliance

Xubo Zhang and Yiyi Zhou

March 16, 2024

Proceedings of the IASS 2024 Symposium
Redefining the Art of Structural Design
August 26-30, 2024, Zurich Switzerland
Philippe Block, Giulia Boller, Catherine DeWolf,
Jacqueline Pauli, Walter Kaufmann (eds.)

Topology optimization of fiber reinforced composite laminates for maximum stiffness

Xubo ZHANG[a], Yiyi ZHOU*

*School of Future Technologies, Hohai University
No.1915 Hehai Avenue, Changzhou 213200, China
Email: 20221275@hhu.edu.cn

[a] College of Mechanics and Materials, Hohai University. No.8 Focheng West Road, Nanjing 211100, China
Email: 15527161395@163.com

Abstract

In this study, a topology optimization technique based on the bi-directional evolutionary structural optimization (BESO) method is developed to maximize the stiffness of fiber reinforced composite laminates. The elastic properties of composite laminates are established and a composite material interpolation scheme is introduced. The effectiveness of the developed BESO method for the composite laminates are verified by three classical examples, namely a cantilever, a Michell-type structure, and an L-bracket. Then, based on the topological results, the topological properties of single-layer composite laminates are presented and compared in detail.

Keywords: Topology optimization; BESO method; fiber reinforced; composite laminate; case study.

1. Introduction

Fiber reinforced composite laminates have been widely used due to the light weight and high strength [1, 2]. For engineering structures, one important demand is to distribute materials appropriately to achieve larger structural stiffness for greater load bearing capacity. Topology optimization performs noticeably well in obtaining essential topology relationship, which can help to achieve this purpose. Therefore, the topology optimization of composite laminates for maximum stiffness has attracted certain attention in the fields where composite laminates are intensively adopted and requirements such as weight reducing or resource saving are critical.

Previous studies in recent decades on the structural optimization of fiber reinforced composites mainly focuses on the optimization of fiber angle, layer sequences and layer thickness [3]. Lund [4] optimized the fiber angles of composite shells to maximize the critical buckling load. The scheme is applied in the design of wind turbine blade. Ma et al. [5] established a optimization framework for maximizing the natural frequency, which could simultaneously optimize the fiber volume, fiber angle and lay sequences of the composite shells.

In the past few years, studies on the topology optimization of fiber reinforced composite laminates gradually increased. Tong et al. [6] conducted the topology optimization of composite laminates to improve the high stress in hinge zones of compliant mechanisms. Bohrer and Kim [7] proposed a three-step scheme based on the lamination parameters and solid isotropic microstructures with penalization (SIMP) method to optimize the topology and layer sequence simultaneously. Duan et al. [8] concurrently optimized the topology and fiber angle of the single-layer using the discrete material optimization and SIMP methods. Wang et al. [9] focused on the stress-based topology optimization of Double-Double (DD) laminates, and proposed a nested p-norm based on the Tsai–Hill failure criterion.

In summary, the current topology optimization of fiber reinforced composites is mainly conducted using the SIMP method. Other topology optimization methods are rarely adopted in this field, their applicability needs to be examined. In the early 1990s, Xie and Steven [10] proposed the evolutionary structural optimization (ESO) method, which was subsequently developed into the bi-directional evolutionary structural optimization (BESO) method [11, 12]. In the last three decades, the ESO/BESO methods have made great progress on several complex problems [13, 14], and been applied in many engineering fields [15, 16]. Therefore, in this study, the topology optimization of the single-layer composite laminates for maximum stiffness is conducted using the BESO method. To extend the BESO method, elastic properties of composite material are presented, and then be penalized by a power function of element density. The BESO scheme for the composite laminates is proposed through this composite material interpolation scheme. The validation of the developed BESO method is verified by three classical numerical cases. The topology results of single-layer laminates are discussed and compared in detail.

2. Elastic properties of composites and the extended BESO method

2.1. Elastic properties

For the plane-stress state, the stress–strain relationship of a single-layer is given by

$$\begin{bmatrix}\sigma_1\\ \sigma_2\\ \tau_{12}\end{bmatrix}=\begin{bmatrix}Q_{11} & Q_{12} & 0\\ Q_{21} & Q_{22} & 0\\ 0 & 0 & Q_{66}\end{bmatrix}\begin{bmatrix}\varepsilon_1\\ \varepsilon_2\\ \gamma_{12}\end{bmatrix}, \tag{1}$$

where "1" denotes the fiber direction, while "2" denotes the direction perpendicular to the fiber. The stiffness matrix $\boldsymbol{Q}$ is determined by the elastic constants of the composite

$$\boldsymbol{Q}=\begin{bmatrix}Q_{11} & Q_{12} & 0\\ Q_{21} & Q_{22} & 0\\ 0 & 0 & Q_{66}\end{bmatrix}=\begin{bmatrix}\dfrac{E_1}{1-\mu_{12}\mu_{21}} & \dfrac{\mu_{12}E_2}{1-\mu_{12}\mu_{21}} & 0\\ \dfrac{\mu_{12}E_2}{1-\mu_{12}\mu_{21}} & \dfrac{E_2}{1-\mu_{12}\mu_{21}} & 0\\ 0 & 0 & G_{12}\end{bmatrix}, \tag{2}$$

E_1, E_2, G_{12}, and μ_{12} are longitudinal modulus, transverse modulus, shear modulus and Poisson ratio of the composite, respectively [17].

Generally, there is a fiber angle θ between the fiber direction and the global coordinate (as shown in Fig. 1 (a)), and the single-layer stress–strain relationship in the global system is

$$\begin{bmatrix}\sigma_x\\ \sigma_y\\ \tau_{xy}\end{bmatrix}=\begin{bmatrix}\bar{Q}_{11} & \bar{Q}_{12} & \bar{Q}_{16}\\ \bar{Q}_{21} & \bar{Q}_{22} & \bar{Q}_{26}\\ \bar{Q}_{16} & \bar{Q}_{26} & \bar{Q}_{66}\end{bmatrix}\begin{bmatrix}\varepsilon_x\\ \varepsilon_y\\ \gamma_{xy}\end{bmatrix}, \tag{3}$$

where the stiffness matrix $\bar{\boldsymbol{Q}}$ in the global system is

$$\bar{\boldsymbol{Q}}=\begin{bmatrix}\bar{Q}_{11} & \bar{Q}_{12} & \bar{Q}_{16}\\ \bar{Q}_{21} & \bar{Q}_{22} & \bar{Q}_{26}\\ \bar{Q}_{16} & \bar{Q}_{26} & \bar{Q}_{66}\end{bmatrix}=\boldsymbol{R}\begin{bmatrix}Q_{11} & Q_{12} & 0\\ Q_{21} & Q_{22} & 0\\ 0 & 0 & Q_{66}\end{bmatrix}\boldsymbol{R}^T. \tag{4}$$

In Eq. (4), $\boldsymbol{R}$ is the rotation matrix and calculated from the fiber angle θ as

$$\boldsymbol{R}=\begin{bmatrix}cos^2\theta & sin^2\theta & -2\,sin\,\theta\,cos\,\theta\\ sin^2\theta & cos^2\theta & 2\,sin\,\theta\,cos\,\theta\\ sin\,\theta\,cos\,\theta & -sin\,\theta\,cos\,\theta & cos^2\theta-sin^2\theta\end{bmatrix}. \tag{5}$$

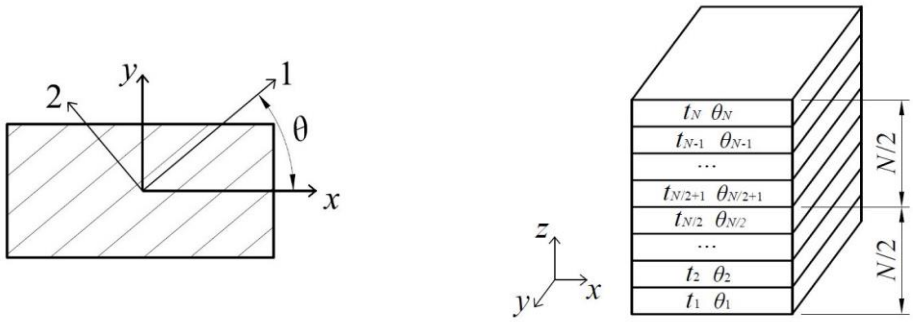

(a) Fiber angle $\boldsymbol{\theta}$ between fiber direction and global coordinate system

(b) Typical laminate structure

Figure 1. Fiber angle and typical structure of composite laminates.

The elastic properties of the composite laminates are calculated by the layers along the thickness. The typical laminate structure is shown in Fig. 1 (b), where the layer number in the composite laminate is N, and the thickness and fiber angle of each layer are t_k and θ_k, respectively. Thus, the constitutive equation of composite laminates is as follows:

$$\begin{bmatrix} \boldsymbol{N} \\ \boldsymbol{M} \end{bmatrix} = \begin{bmatrix} \boldsymbol{A} & \boldsymbol{B} \\ \boldsymbol{B} & \boldsymbol{D} \end{bmatrix} \begin{bmatrix} \boldsymbol{\varepsilon_0} \\ \boldsymbol{\kappa} \end{bmatrix}, \tag{6}$$

where, $\boldsymbol{N}$ and $\boldsymbol{M}$ are the internal force and moment resultants, respectively; $\boldsymbol{A}$, $\boldsymbol{B}$, and $\boldsymbol{D}$ are the in-plane tensional, tension-bending coupling, and bending material stiffness matrices, respectively; $\boldsymbol{\varepsilon_0}$ and $\boldsymbol{\kappa}$ are the mid-plane strains and curvatures, respectively. $\boldsymbol{A}$, $\boldsymbol{B}$, and $\boldsymbol{D}$ matrixes are calculated by the properties of all single-layers:

$$\begin{aligned} A_{ij} &= \sum_{k=1}^{N} \bar{Q}_{ij}^{k} \left(z_k - z_{k-1}\right) (i,j = 1,2,6) \\ B_{ij} &= \frac{1}{2} \sum_{k=1}^{N} \bar{Q}_{ij}^{k} \left(z_k^2 - z_{k-1}^2\right) (i,j = 1,2,6) \\ D_{ij} &= \frac{1}{3} \sum_{k=1}^{N} \bar{Q}_{ij}^{k} \left(z_k^3 - z_{k-1}^3\right) (i,j = 1,2,6) \end{aligned} \tag{7}$$

When the laminated layers are symmetric, matrix $\boldsymbol{B} = \boldsymbol{0}$, which indicates that tension and bending are not coupled. Thus, the symmetric laminates are more widely used in engineering.

2.2. Material interpolation scheme

Material interpolation scheme with penalization has been widely used in the SIMP method [35]. According to the basic idea of the SIMP method, the elastic constants of the intermediate composite material are given as

$$\begin{bmatrix} E_1(x_i) \\ E_2(x_i) \\ G_{12}(x_i) \end{bmatrix} = x_i^p \begin{bmatrix} E_1 \\ E_2 \\ G_{12} \end{bmatrix}, \tag{8}$$

where, E_1, E_2, and G_{12} denote the elastic constants of the solid composite material; p is the penalty coefficient, which is often preset as 3. Substituting Eq. (8) into Eq. (1)-(7), the penalized material stiffness is calculated as

$$\begin{bmatrix} \boldsymbol{A}(x_i) \\ \boldsymbol{B}(x_i) \\ \boldsymbol{D}(x_i) \end{bmatrix} = x_i^p \begin{bmatrix} \boldsymbol{A} \\ \boldsymbol{B} \\ \boldsymbol{D} \end{bmatrix}. \tag{9}$$

This indicates that the penalty on the elastic constants will eventually turn into the penalty on $\boldsymbol{A}$, $\boldsymbol{B}$, and $\boldsymbol{D}$ matrices.

2.3. BESO scheme for fiber reinforced composite laminates

In this study, the BESO method is developed to achieve the topology optimization of composite laminates using the material interpolation scheme Eq. (9). The scheme and process are illustrated in this section.

2.3.1 Problem statement

In the BESO method, the finite element analysis (FEA) is used and binary design variables are introduced. Therefore, the optimization model for maximizing structural stiffness with the volume constraint is stated as

$$\begin{cases} \text{find} \quad \boldsymbol{x} = [x_1, x_2, x_3, \dots, x_n]^T \\ \min \quad C = \dfrac{1}{2} \cdot \boldsymbol{F}^T \boldsymbol{U} \\ \text{s.t.} \quad V^* - \displaystyle\sum_{i=1}^{n} V_i \cdot x_i = 0 \\ \boldsymbol{K}\boldsymbol{U} = \boldsymbol{F} \\ x_i = 1 \ (\text{solid}) or \ x_{min} \ (\text{void}) \end{cases} . \tag{10}$$

Where, x_i is the binary design variable of each element; C is the compliance of the structure; $\boldsymbol{K}$, $\boldsymbol{U}$, and $\boldsymbol{F}$ are the global stiffness, displacement and external loads, respectively; V^* is the preset volume of final structure; V_i is the volume of each element; x_{min} is a minimum preventing the singularity of structure stiffness matrix, and often preseted as 0.001.

2.3.2 Sensitivity number

The sensitivity number in the BESO method is defined by the sensitivity ranking of the objective function. The sensitivity is given as [11]

$$\frac{dC}{dx_i} = -\frac{1}{2} \boldsymbol{U}^T \frac{d\boldsymbol{K}}{dx_i} \boldsymbol{U}. \tag{11}$$

Substituting the material interpolation schemes Eq. (9) into Eq. (11), the sensitivity becomes

$$\frac{\partial C}{\partial x_i} = -\frac{1}{2} p x_i^{p-1} \boldsymbol{u_i}^T \boldsymbol{k_0} \boldsymbol{u_i}, \tag{12}$$

where, $\boldsymbol{k_0}$ is the elemental stiffness matrix of the solid elements; $\boldsymbol{u_i}$ is the nodal displacement vector of the element. According to the FEA procedure, $\boldsymbol{k_0}$ is written as

$$\boldsymbol{k_0} = \int \boldsymbol{B_e}^T \boldsymbol{C_0} \boldsymbol{B_e}, \tag{13}$$

where, $\boldsymbol{C_0}$ represents matrices $\boldsymbol{A}$, $\boldsymbol{B}$, and $\boldsymbol{D}$ of the solid composite material; $\boldsymbol{B_e}$ is the strain-displacement matrix.

Therefore, the sensitivity number in the BESO method is

$$\alpha_i = -\frac{1}{p} \frac{\partial C}{\partial x_i} = \frac{1}{2} x_i^{p-1} \boldsymbol{u_i}^T \boldsymbol{k_0} \boldsymbol{u_i}. \tag{14}$$

Due to the binary design variable, Eq. (14) is finally written as

$$\alpha_i = \begin{cases} \frac{1}{2}\boldsymbol{u_i^T k_0 u_i} & if\ x_i = 1\ \text{(soild)} \\ \frac{1}{2}x_{min}^{p-1}\boldsymbol{u_i^T k_0 u_i} & if\ x_i = x_{min}\ \text{(void)} \end{cases}. \tag{15}$$

2.3.3 Filter scheme

The checkerboard and mesh-dependency problems are two common numerical instabilities[11], which can be avoided by filter schemes. Here, the sensitivity filter scheme is adopted as

$$\alpha_i' = \frac{\sum_{j=1}^{M}\omega(r_{ij})\alpha_j}{\sum_{j=1}^{M}\omega(r_{ij})}, \tag{16}$$

where, M is the total number of all elements whose geometric centers within the circular region of filter radius r_{min}; r_{ij} indicates the straight distance between the center of the j-th element in the circular region and the center of the i-th element of the entire design domain; $\omega(r_{ij})$ is the weight coefficient of the elements in the region and written as

$$\omega(r_{ij}) = r_{min} - r_{ij} \quad (j = 1,2,\dots,M). \tag{17}$$

Furthermore, to stabilize the evolutionary process, the sensitivity number is averaged with its historical information:

$$\bar{\alpha}_i^q = \frac{1}{2}(\alpha_i^q + \alpha_i^{q-1}) \quad (q \geq 2), \tag{18}$$

where, q is the current iteration step; α_i^{q-1} is the sensitivity number of the i-th element in the previous iteration step; α_i^q and $\bar{\alpha}_i^q$ are the sensitivity numbers before and after averaged.

2.3.4 Element removal/addition and convergence criteria

Before removing/adding elements in the BESO method, the target volume V_q needs to be determined. The V_q is gradually reduced with a certain evolutionary volume ratio ER until the volume constraint V^* is reached. Thus the V_q is given as

$$V_q = max(V_{q-1}(1 - ER), V^*). \tag{19}$$

Elements are added and removed according to the ranking of sensitivity numbers, and the threshold $\bar{\alpha}_{th}$ is determined by the V_q. For solid element with $x_i = 1$, if

$$\bar{\alpha}_i^q \leq \bar{\alpha}_{th}, \tag{20}$$

it will be removed with x_i switched to x_{min}. Similarly, for void element, if

$$\bar{\alpha}_i^q > \bar{\alpha}_{th}, \tag{21}$$

it will be added with x_i switched from x_{min} to 1.

Then, to determine the convergence of the optimization process, the compliance in each iteration step C_q is calculated. The following convergence criterion is adopted:

$$\frac{\left|\sum_{h=1}^{L} C_{q-h+1} - \sum_{h=1}^{L} C_{q-L-h+1}\right|}{\sum_{h=1}^{L} C_{q-h+1}} \leq \xi, \tag{22}$$

where, q is the current iteration step; ξ is the allowable convergence tolerance; L is an integer. L is often preset as 5, thus Eq. (22) indicates that the change in the compliance over the last 10 iterations is acceptably small.

2.3.5 BESO process

Therefore, the BESO process of the composite laminates for maximum structural stiffness is given as follows:

(1) Define the design domain using a finite element mesh and assign all initial variables equal to 1.

(2) Define the BESO parameters: V^*, ER, p, r_{min}, ξ.

(3) **Loop** over design iterations:

(a) determine the target volume of current iteration according to Eq. (19).

(b) perform finite element analysis using the current topology shape

(c) calculate the sensitivity numbers according to Eq. (15).

(d) filter and average the sensitivity numbers using Eq. (16) and (18).

(e) add and delete elements by updating topology variables.

(f) repeat (a)-(e) until the preset volume V^* is reached and the convergence criterion is satisfied.

(4) **End**.

3. Numerical case study

In this section, numerical cases are used to validate the effectiveness of the development of the BESO method on the topology optimization of composite laminates for the maximum stiffness. Then, the topological performances of single-layer composite laminates are investigated in detail.

3.1 Material and case illustration

The single-layer of T300/epoxy product is adopted. Its properties are shown in Tab. 1 [4].

Table 1. Properties of T300/epoxy product [4].

Property	E_1 (GPa)	E_2 (GPa)	G_{12} (GPa)	μ_{12}	ρ (g/cm^3)
Value	135	10	5	0.27	1.58

In research on the continuum topology optimization, the common numerical examples include the cantilever, Michell-type structure, L-bracket, etc. Among them, cantilever case, whose stress state and internal balance are relatively clear, is often used to check the newly proposed methods and algorithms, such as the multi-material design optimization with different tension and compression properties [13], and stress-based or stress constraint topology optimization scheme [18]. The Michell-type structure has less restraint in forming than the cantilever, and its topological shape at the final stage tends to be a Michell-truss (shown in Fig. 2) [11]. The L-bracket introduces stress concentration, which is usually used in stress-based or stress constraint topology optimization scheme [9, 18] and multi-material design optimization [19].

Therefore, the topology optimization is studied based on a cantilever, a Michell-type structure, and an L-bracket here. For the single-layer composite laminates, the fiber angles are taken as the study object and its concurrent effects with topological shapes on compliance are investigated. Three examples are shown in Fig. 3 (a)-(c).

(a) Loading and boundary conditions (b) Optimized topology

Figure 2. A Michell-type structure [6].

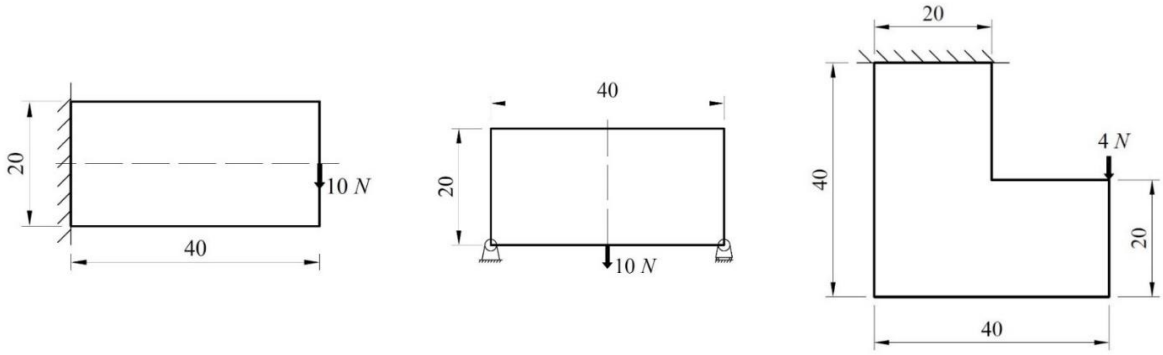

(a) Cantilever (b) Michell-type structure (c) L-bracket

Figure 3. Three classical numerical cases.

The BESO parameters of all examples are preset as: $ER = 1\%$, $V^* = 50\%$, $\xi = 0.01\%$, $p = 3$, and r_{min} is 3 times of the element size.

3.2 Cantilever case

3.2.1 Influence of mesh density

Taking the single-layer with 45° fiber angle as an example, the compliance of various mesh densities is investigated, then the maximum element size can be confirmed. The numbers of elements are taken as 60×30, 80×40, 100×50, and 120×60. The final shapes and compliance are shown in Fig. 4 and Tab. 2. It shows that, with the increase of mesh density, the compliance decreases at first and then becomes stable. The maximum element size for stable compliance is 0.5 mm. Therefore, the mesh densities in subsequent studies will be determined by the maximum element size and computation costs.

(a) 60×30. (b) 80×40. (c) 100×50. (d) 120×60.

Figure 4. Topological shape of cantilever case with different mesh densities.

Table 2. Compliance of cantilever case with different mesh densities.

Mesh density	60×30	80×40	100×50	120×60
Compliance (N · mm)	0.7387	0.7103	0.7103	0.7144

3.2.2 Influence of fiber angle

Fiber angles of 0° to 90° at an internal of 15° are considered. A mesh density of 100×50 meeting the element size requirement is adopted. The compliance is presented in Fig. 5. Due to the symmetry, the results of a negative fiber angle are symmetrical up and down with those obtained by its opposite fiber angle, and thus are not presented. From Fig. 5, fiber angle is the main factor affecting compliance in the cantilever case. As fiber angle increases, the compliance increases.

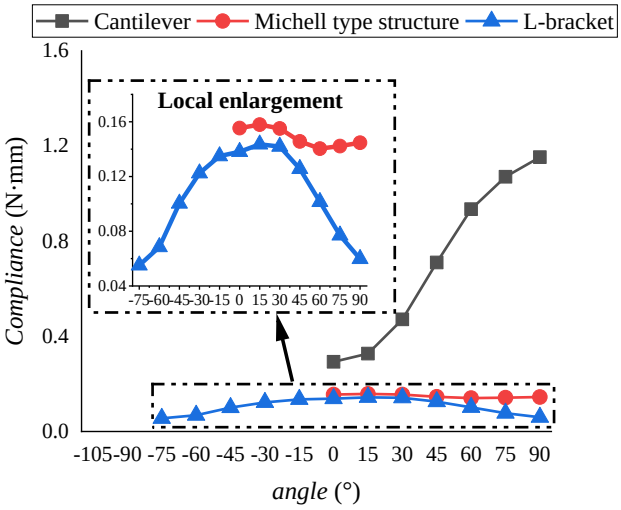

Figure 5. Compliance of cantilever case with different fiber angles.

The reason that compliance changes with fiber angles changing is investigated through the stress distribution, as displayed in Fig. 6, where "S_1" and "S_2" denotes the stress along the 1-direction and 2-direction respectively. In Fig. 6, for the 0° angle, the external load is mainly borne by E_1 with extremely small S_2. For the 45° angle, the load is borne by E_1 and E_2. For the 90° angle, the load is mainly borne by E_2 with extremely small S_1. This indicates that, as the fiber angle increases, the stress in 2-direction gradually becomes the dominance and the smaller transverse modulus E_2 gradually works. Thus, the compliance increases accordingly. It also shows that the cantilever case has more restraint in forming with more defined topology, and the compliance is mainly affected by the fiber angle.

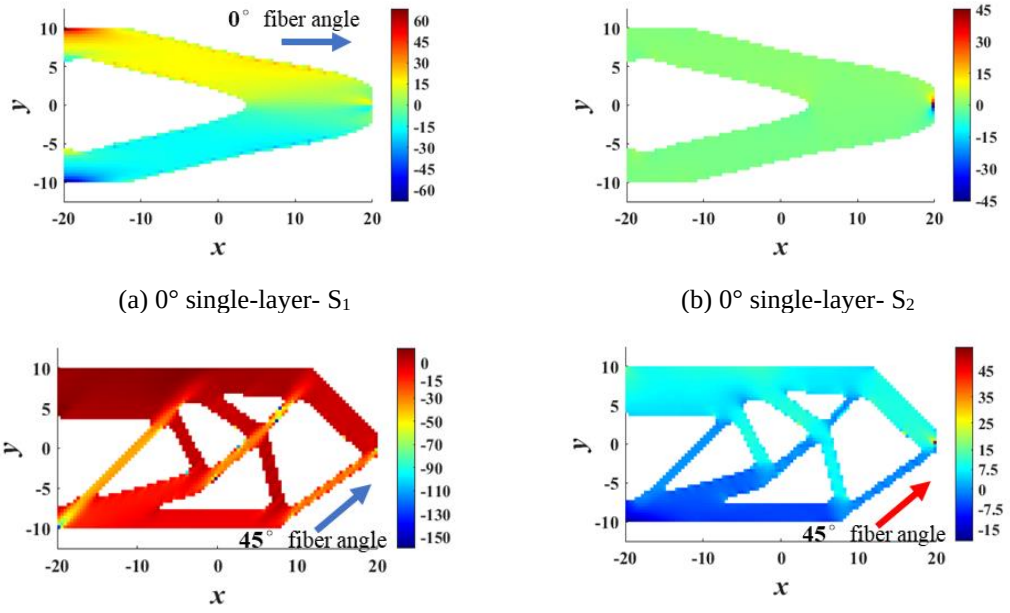

(a) 0° single-layer- S_1

(b) 0° single-layer- S_2

(c) 45° single-layer- S_1

(d) 45° single-layer- S_2

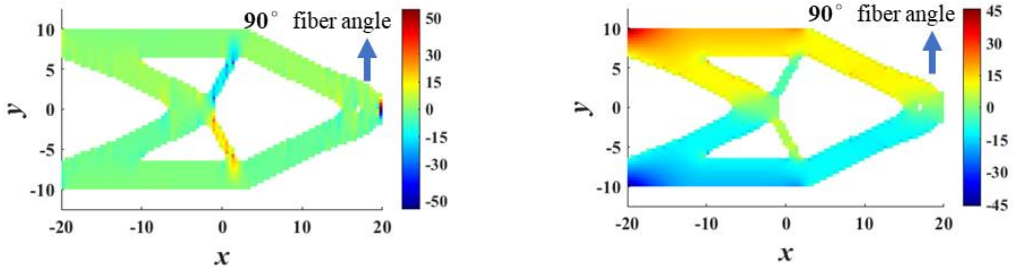

(e) 90° single-layer- S_1 (f) 90° single-layer- S_2

Figure 6. Stress distribution of cantilever case with different fiber angles.

3.2 Michell- type structure case

Again, a mesh density of 100×50 is adopted. The fiber angles of 0° to 90° at an internal of 15° are preseted. The Michell-type structure is symmetric, and the results of a negative fiber angle condition are thus not presented either.

The compliance of single-layers is shown in Fig. 5. Since this case has only two constraint nodes and one loading point, the structure has less restraint in forming. The relationship between the compliance and fiber angle is more complex.

The variation of compliance is also analyzed by stress distribution (displayed in Fig. 7). It should be noted that the internal and external forces need to be balanced in final structure, and the internal tension and compression also need to be balanced. To maximize load bearing efficiency and reduce compliance, the final topological structure should be similar to a Michell-truss (shown in Fig. 2).

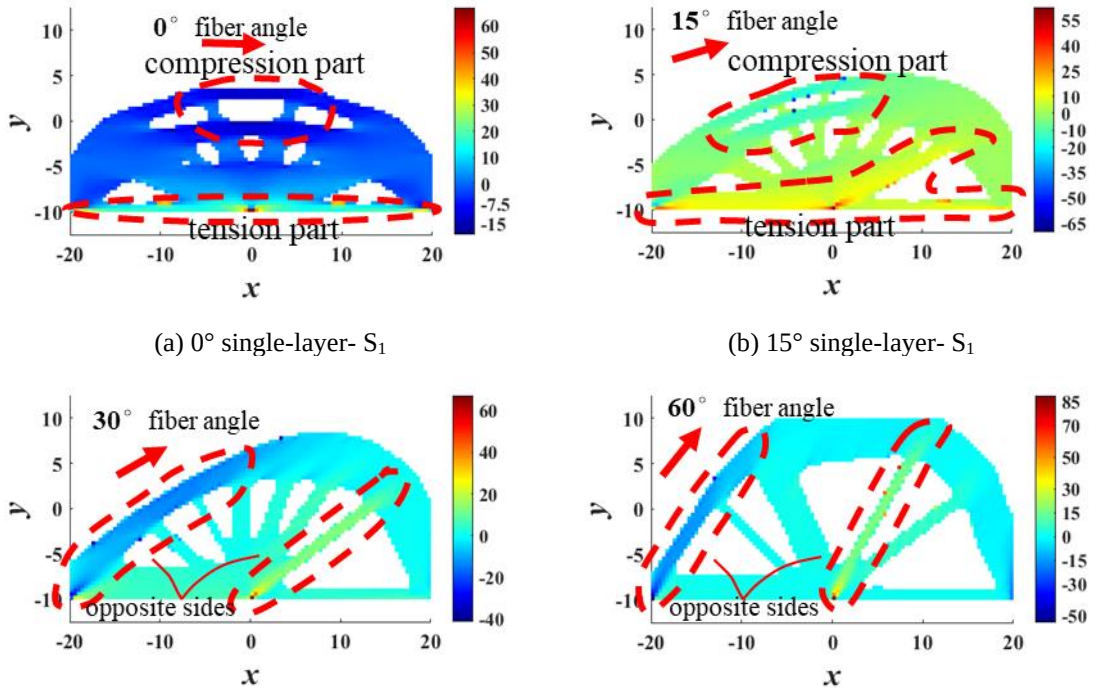

(a) 0° single-layer- S_1 (b) 15° single-layer- S_1

(c) 30° single-layer- S_1 (d) 60° single-layer- S_1

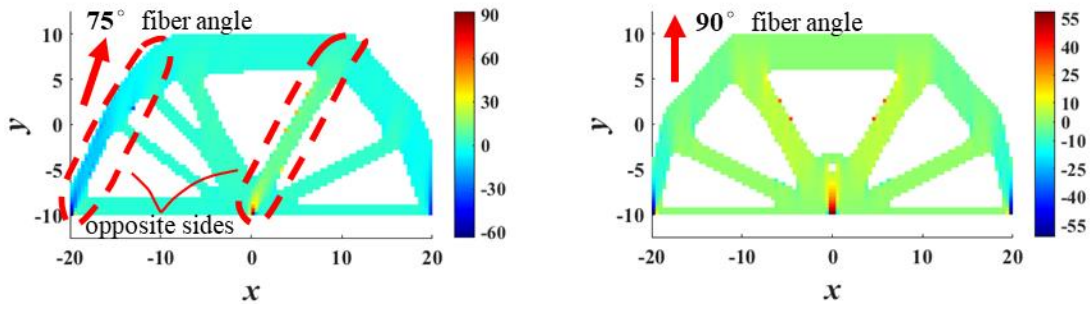

(e) 75° single-layer- S_1 (f) 90° single-layer- S_1

Figure 7. Stress distribution of Michell-type structure case with different fiber angles.

From Fig. 7 (c)-(e), for 30° to 60° fiber angles, the internal tension-compression balance and force path are clear. The external force is mainly borne by a pair of tension-compression balanced opposite sides along fiber direction with uniform stress (similar to bar elements), while stress in the rest parts is small. Thus, the load bearing efficiency is improved, and the compliance is less. Due to the internal and external balance, as fiber angles increase, the opposite sides are closer to the external force direction. Internal forces of the sides decrease with a thinner shape. This induces gradually decreased compliance for 30° to 60° fiber angle conditions. For 75° fiber angle, the opposite sides are inclined to fiber direction. The load bearing efficiency decreases with larger compliance compared with the 60° single-layer.

For the single-layers with rest fiber angles, force paths are not clear. Vast elements in middle part are in low stress state to transmit stress. This induces low load bearing efficiency and large compliance.

Summarily, for the Michell-type structure case, due to the more freedom in forming, the compliance is affected by the fiber angles and topological shapes. Clear force paths benefit the load bearing efficiency. To be specific, when there are opposite sides with uniform tension and compression along fiber direction, the load bearing efficiency is improved and the compliance is accordingly reduced.

3.3 L-bracket case

The L-bracket is asymmetric and introduces stress concentration. Therefore, fiber angles of -75° to 90° at an interval of 15° are all considered, and the mesh density is set as 80×80.

The compliance of the L-bracket is listed in Fig. 5. With the increase of fiber angle, the compliance first increases and then decreases. To analyze the variation of compliance, stress distribution of single-layers is presented in Fig. 8.

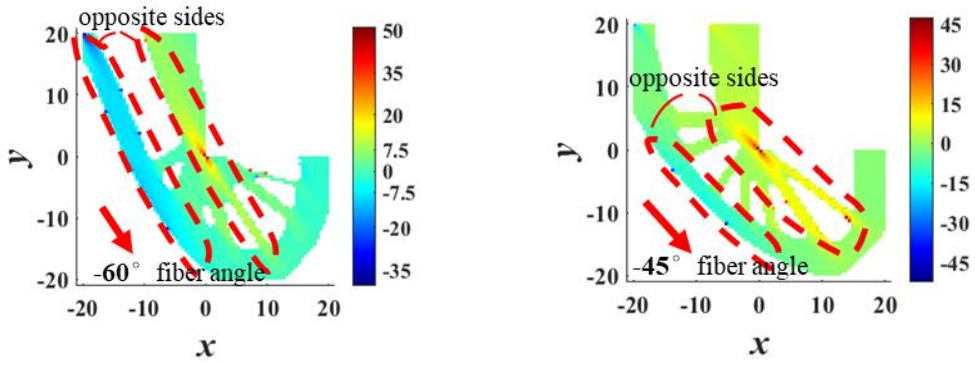

(a) -60° single-layer- S_1 (b) -45° single-layer- S_1

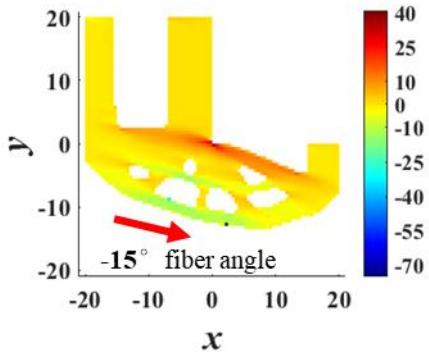

(c) -15° single-layer- S_1

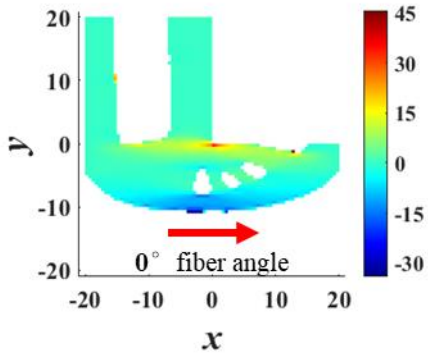

(d) 0° single-layer- S_1

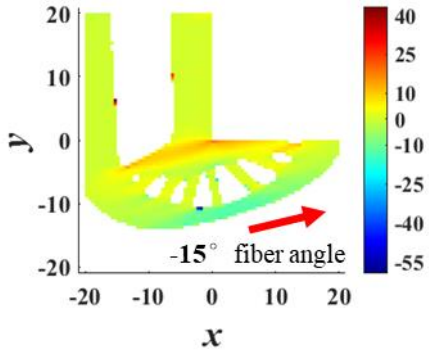

(e) 15° single-layer- S_1

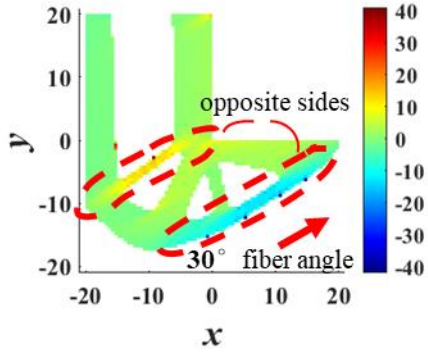

(f) 30single-layer- S_1

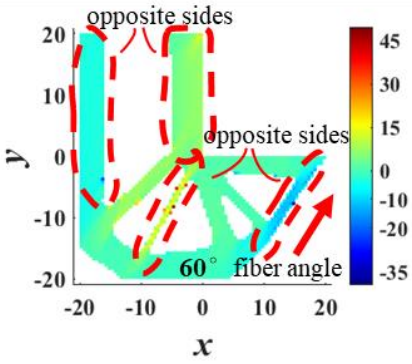

(g) 60° single-layer- S_1

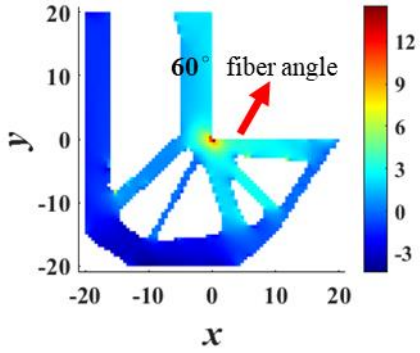

(h) 60° single-layer- S_2

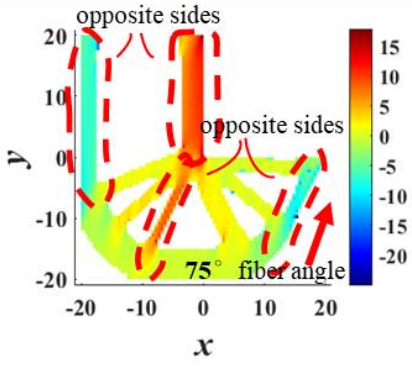

(i) 75° single-layer- S_1

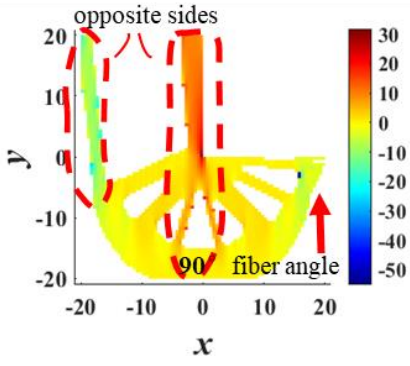

(j) 90° single-layer- S_1

Figure 8. Stress distribution of L-bracket case with different fiber angles.

From Fig. 8 (a)-(b), for -75° to -30° fiber angles, the internal tension-compression balance is clear and established by a pair of balanced opposite sides along fiber direction. Due to the geometry of L-bracket, opposite sides in the -75° and -60° single-layers are directly connected to supports with fewer elements in intermediate stress state. Thus, the compliance of -75° and -60° fiber angle conditions is lower. From -75° to -30°, the fiber angle gradually deviates from the external force direction, and elements transmitting stress increases. Therefore, the compliance increases. Additionally, the stress concentration in this condition is mainly borne by E_1, i.e. by fibers.

From Fig. 8 (c)-(e), for -15° to 15° fiber angles, the stress in most areas of the final topological structure is close (except stress concentration area). There are no clear force paths in these single-layers. The transversal modulus E_2 gradually involved. These induces low load bearing efficiency, thus the compliance increases.

From Fig. 8 (f)-(j), for 30° to 90° fiber angles, force paths and opposite sides are re-clear. The fiber angle is gradually closer to the external force direction, inducing gradually decreased compliance. In the 60° and 75° single-layers, another pair of opposite sides connected with supports appear. While in the 90° single-layer, two opposite sides are integrated and completely along the external force direction. Due to the L-bracket geometry, stress concentration in this condition is mainly borne by E_2 (as shown in Fig. 20 (h)), and elements transmitting stress are more compared with the corresponding opposite angle conditions. Thus, the compliance for the positive fiber angle is larger.

In aggregate, the L-bracket and Michell-type structure cases have similar topology properties. The compliance is affected by fiber angles and topological shapes together. When force paths are clear, the load bearing efficiency is enhanced with lower compliance. Due to the larger longitudinal modulus E_1, the stress concentration borne by fibers can also induce lower compliance.

4. Conclusion

In this study, a topology optimization technique based on the BESO method is developed to maximize the stiffness of fiber reinforced composite laminates. The conclusions are as follows:

(1) By means of the composite material interpolation scheme, an extended BESO method is proposed for the topology optimization of fiber reinforced composite laminates. Through three numerical cases, the developed BESO method is verified to be efficient in the topology optimization of single-layer composite laminates for the maximum stiffness. It is identified as an effective technique to analyze the topological properties of composite laminates.

(2) Through the cantilever case, the effect of fiber angles is analyzed. When structure has less freedom in forming, the fiber angle is the main factor affecting compliance. In this case, as the fiber angle increases, the compliance increases accrodingly due to the transverse modulus gradually working.

(3) Through the Michell-type structure and L-bracket cases, the concurrent effect of topological shapes and fiber angles on the compliance is analyzed. Low compliance is the result of clear and direct force paths. When there are opposite sides with uniform tension and compression in fiber direction (similar to bar elements), corresponding load bearing efficiency is enhanced. If stress concentration is borne by the fibers, the compliance will also decrease.

References

[1] Siwowski T., Kulpa M., Rajchel M., Poneta P., Design, manufacturing and structural testing of all-composite FRP bridge girder. *Composite Structures*, 2018; **206**; 814-827.

[2] Monfared V., Ramakrishna S., Alizadeh A., Hekmatifar M., A systematic study on composite materials in civil engineering. *Ain Shams Engineering Journal*, 2023; **14(12)**; 102251.

[3] Xu Y., Zhu J., Wu Z., Cao Y., Zhao Y., Zhang W., A review on the design of laminated composite structures: constant and variable stiffness design and topology optimization. *Advanced Composites and Hybrid Materials*, 2018; **1**; 460–477.

[4] Lund E., Buckling topology optimization of laminated multi-material composite shell structures. *Composite Structures*, 2009; **91(2)**; 158-167.

[5] Ma X., Tian K., Li H., Zhou Y., Hao P., Wang B., Concurrent multi-scale optimization of hybrid composite plates and shells for vibration. *Composite Structures*, 2020; **233**; 111635.

[6] Tong X., Ge W., Sun C., Liu X., Topology optimization of compliant adaptive wing leading edge with composite materials. *Chinese Journal of Aeronautics*, 2014; **27(6)**; 1488-1494.

[7] Bohrer R.Z. and Kim Y., Concurrent topology and stacking sequence optimization of composite laminate plates using lamination parameters. *Composite Structures*, 2021; **276**; 114556.

[8] Duan Z., Liu Y., Fan J., Long K., Xu B., Zhu J., Yan J., Concurrent multi-material and multi-scale design optimization of fiber-reinforced composite material and structures for minimum structural compliance. *Composite Structures*, 2023; **311**; 116796.

[9] Wang Y., Wang D., Zhong Y., Li S., Tsai S.W., Topology optimization of Double-Double (DD) composite laminates considering stress control. *Computer Methods in Applied Mechanics and Engineering*, 2023; 414; 116191.

[10] Xie Y.M. and Steven G.P., A simple evolutionary procedure for structural optimization. *Computers & Structures*, 1993; **49(5)**; 885-896.

[11] Huang X and Xie Y.M., Evolutionary topology optimization of continuum structures: Methods and applications. Chichester; John Wiley & Sons Ltd, 2010.

[12] Querin O.M., Steven G.P., Xie Y.M., Evolutionary Structural Optimization using an additive algorithm. *Finite Elements in Analysis and design*, 2000; **34**; 291-308.

[13] Li Y. and Xie Y.M., Evolutionary topology optimization for structures made of multiple materials with different properties in tension and compression. *Composite Structures*, 2021; **259**; 113497.

[14] Xu T., Huang X., Lin X., Xie Y.M., Topology optimization for maximizing buckling strength using a linear material model. *Computer Methods in Applied Mechanics and Engineering*, 2023; **417**; 116437.

[15] Lai Y., Li Y., Huang M., Zhao L., Chen J., Xie Y.M., Conceptual design of long span steel-UHPC composite network arch bridge. *Engineering Structures*, 2023; **277**; 115434.

[16] Li Y., Ding J., Zhang Z., Zhou X., Makvandi M., Yuan P.F., Xie Y.M., Practical application of multi-material topology optimization to performance-based architectural design of an iconic building. *Composite Structures*, 2023; **325**; 117603.

[17] Banerjee S. and Sankar B.V., Mechanical properties of hybrid composites using finite element method based micromechanics. *Composites Part B: Engineering*, 2014; **58**; 318-327.

[18] Xia L., Zhang L., Xia Q., Shi T., Stress-based topology optimization using bi-directional evolutionary structural optimization method. *Computer Methods in Applied Mechanics and Engineering*, 2018; **333**; 356-370.

[19] Lee J.W., Kim J.J., Yoon G.H., Stress constraint topology optimization using layerwise theory for composite laminates. *Composite Structures*, 2019; **226**; 111184.